Dalton Transactions

ARTICLE

O–H Bond Oxidation by a Monomeric Mn^{III}–OMe Complex

Gayan B. Wijeratne, Victor W. Day, and Timothy A. Jackson*

Manganese-containing, mid-valent oxidants (Mn^{III}–OR) that mediate proton-coupled electron-transfer (PCET) reactions are central to a variety of crucial enzymatic processes. The Mn-dependent enzyme lypoxygenase is such an example, where a Mn^{III}–OH unit activates fatty acid substrates for peroxidation by an initial PCET. This present work describes the quantitative generation of the Mn^{III}–OMe complex, [Mn^{III}(OMe)(dpaq)]$^+$ (dpaq = 2-[bis(pyridin-2-ylmethyl)]amino-N-quinolin-8-yl-acetamidate) via dioxygen activation by [Mn^{II}(dpaq)]$^+$ in methanol at 25 ℃. The X-ray diffraction structure of [Mn^{III}(OMe)(dpaq)]$^+$ exhibits a Mn–OMe group, with a Mn–O distance of 1.825(4) Å, that is *trans* to the amide functionality of the dpaq ligand. The [Mn^{III}(OMe)(dpaq)]$^+$ complex is quite stable in solution, with a half-life of 26 days in MeCN at 25 ℃. [Mn^{III}(OMe)(dpaq)]$^+$ can activate phenolic O–H bonds with bond dissociation free energies (BDFEs) of less than 79 kcal/mol and reacts with the weak O–H bond of TEMPOH (TEMPOH = 2,2'-6,6'-tetramethylpiperidine-1-ol) with a hydrogen/deuterium kinetic isotope effect (H/D KIE) of 1.8 in MeCN at 25 ℃. This isotope effect, together with other experimental evidence, is suggestive of a concerted proton-electron transfer (CPET) mechanism for O–H bond oxidation by [Mn^{III}(OMe)(dpaq)]$^+$. A kinetic and thermodynamic comparison of the O–H bond oxidation reactivity of [Mn^{III}(OMe)(dpaq)]$^+$ to other M^{III}–OR oxidants is presented as an aid to gain more insight into the PCET reactivity of mid-valent oxidants. In contrast to high-valent counterparts, the limited examples of M^{III}–OR oxidants exhibit smaller H/D KIEs and show weaker dependence of their oxidation rates on the driving force of the PCET reaction with O–H bonds.

Introduction

Manganese-dependent enzymes that mediate proton coupled electron transfer (PCET) reactions perform vital processes in humans and numerous other organisms.[1] PCET reactivity within the tetranuclear manganese active site of the oxygen evolving complex (OEC) of photosystem II represents a classic example. This active-site cluster consists of a Mn$_3$CaO$_4$ cubane with a dangler Mn atom linked to the cubane by oxo bridges.[2] In the most recent crystal structure, the cluster is capped with four terminal water ligands.[2] During the oxidation of the OEC from its least oxidized S$_0$ state to the most oxidized S$_4$ state, coordinated water molecules within the cluster have been proposed to be deprotonated as a part of sequential PCET processes, producing reducing equivalents. [2-6] In light of this proposal, as well as numerous other biological examples of metal-mediated PCET,[7, 8] model complexes that can facilitate PCET have been extensively studied to understand the thermodynamics and kinetics of these processes.[9-17]

In general, PCET reactions can be categorized as concerted or sequential, based on whether the proton and electron are being transferred in a single step or multiple steps, respectively.[18] Single-step processes where the proton and electron share the same orbital/bond following the reaction are often referred to as hydrogen atom (H$^{\bullet}$ = H$^+$ + e$^-$) transfer (HAT) reactions. This is a common reaction in organic chemistry, and has been the subject of numerous detailed studies over the past century.[13] On the other hand, when transition metal complexes are involved, most often the proton and electron are transferred to separate entities (*i.e.* a ligand and the metal), and no longer share the same bond. These metal-mediated PCET reactions can also occur either in a single (concerted proton-electron transfer; CPET) or multiple (proton transfer followed by electron transfer or *vice versa*; PT/ET or ET/PT) kinetic steps.[19] Synthetic transition metal complexes that can facilitate PCET reactions are of great interest not only because they mimic metalloenzyme reactions, but also because PCET is central to many industrial processes.[1] Recently, more work has been focused on developing PCET mediators using

greener, less expensive metals, such as high-valent and mid-valent manganese and iron complexes.[20-29] High-valent (M^{IV} or M^V; M = Mn or Fe) oxidants, typically containing terminal oxo ligands, have been the subject of a large number of studies, as these exhibit efficient reactivity with stronger, unactivated C–H or O–H bonds.[20-24] In contrast, only several examples of mid-valent metal (M^{III}) oxidants have been reported to-date,[25-29] although these compounds exhibit unique reactivity patterns that can be used to gain detailed understanding into the fundamental thermodynamic and kinetic parameters that govern PCET reactions. Among the mid-valent oxidants reported, M^{III}–OR (M = Mn or Fe; R = H, CH_3, Ph) species are the most common. In PCET reactions with M^{III}–OR species, M^{II}–O(H)R is generated as the final metal based product (Scheme 1).
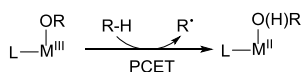
Scheme 1. PCET reactivity of a mid-valent oxidant (M^{III}–OR) with an H• donor substrate (R–H, where R is C or O).

The principal thermodynamic parameters controlling PCET reactivity are the reduction potential of the oxidized metal center (E^o) and the acidity of the reduced product (*i.e.*, the pK_a of the M^{II}–O(H)R species).[13] The relationship between these values and the free energy change of the reaction (ΔG) is described by the Bordwell relationship ($\Delta G^o = -23.06E^o - 1.37pK_a - C$).[10, 30] This relationship can, in principle, be applied to the design of better oxidants as both the reduction potential and pK_a parameters are tunable by the ligand framework. E^o can be controlled through the electronic properties of the supporting and –OR ligands and the pK_a results from a combination of supporting ligand effects and intrinsic properties of the M^{II}–O(H)R group. In this regard, variation of the R group of mid-valent M–OR oxidants has the potential to tune PCET reactivity by a means unavailable for high-valent M=O species. However, given the limited examples of mid-valent M–OR oxidants with different R groups,[25, 27, 28] it is difficult to elaborate broadly on how ligand properties affect the thermodynamic and kinetic properties of the oxidant, and how these can be modified to design better PCET mediators.
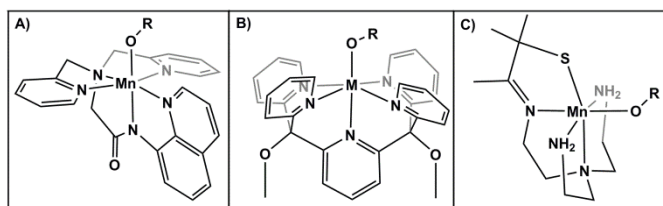
Figure 1. Representative Structures for PCET Mediating M^{III}–OR Adducts of A) $[Mn^{III}(OR)(dpaq)]^+$,[29] B) $[M^{III}(OR)(PY5)]^{+}$,[26] and C) $[Mn^{III}(OR)(S^{Me2}N_4(tren))]^{+}$[25] series of complexes.

Current examples of PCET-mediating M^{III}–OR complexes with multiple R groups are found in the $[Mn^{III}(OH)(S^{Me2}N_4(tren))]^+$ and $[Mn^{III}(OMe)(S^{Me2}N_4(tren))]^+$ complexes of Kovacs and co-workers ($S^{Me2}N_4(tren)$ = 3-((2-

(bis(2-aminoethyl)amino)ethyl)imino)-2-methylbutane-2-thiolate),[25] and the $[M^{III}(OH)(PY5)]^{2+}$ and $[M^{III}(OMe)(PY5)]^{2+}$ complexes of Stack and Goldsmith (M = Mn and Fe; PY5 = 2,6-bis(bis(2-pyridyl)methoxymethane)pyridine) (Figure 1).[26-28] The change in thermodynamic properties as a function of the –OR group can be clearly seen in the experimental E^o values of the $[Mn^{III}(OR)(S^{Me2}N_4(tren))]^+$ series (Figure 1; R = H, –OMe, –OPh and –OPh$^{p-NO_2}$).[25] The $[Mn^{III}(OPh^{p-NO_2})(S^{Me2}N_4(tren))]^+$ complex, with the most electron-withdrawing –OPh$^{p-NO_2}$ ligand, displayed the highest E^o along with the lowest pK_a. In contrast, $[Mn^{III}(OH)(S^{Me2}N_4(tren))]^+$, with one of the most electron-donating –OR ligands, showed the lowest E^o and highest pK_a.[25] Thus, in this series, E^o and pK_a display an inverse correlation. As a net result, only $[Mn^{III}(OH)(S^{Me2}N_4(tren))]^+$ and $[Mn^{III}(OMe)(S^{Me2}N_4(tren))]^+$ showed the ability to oxidize the weak O–H bond of TEMPOH, with similar second-order rate constants of 2.1×10^3 M^{-1} s^{-1} and 3.6×10^2 M^{-1} s^{-1}, respectively. The other two Mn^{III}–OR species with the most electron-withdrawing –OR ligands were inert toward TEMPOH. Therefore, it was concluded that under similar entropic factors, the more electron-withdrawing $[Mn^{III}(OPh^{p-NO_2})(S^{Me2}N_4(tren))]^+$ and $[Mn^{III}(OPh)(S^{Me2}N_4(tren))]^+$ did not have a sufficiently large E^o to overcome the substantially small pK_a to provide the requisite driving force for PCET.[25] In the Mn^{III} and Fe^{III} complexes of Stack and Goldsmith (Figure 1), interesting trends are evident when comparing the Mn versus Fe complexes, where $[Mn^{III}(OH)(PY5)]^{2+}$ was found to be the overall best oxidant of the series, with the highest E^o and pK_a.[28]

This present work describes the formation and PCET reactivity of the new complex $[Mn^{III}(OMe)(dpaq)]^+$, which is formed in quantitative yields when $[Mn^{II}(dpaq)]^+$ is reacted with dioxygen in methanol at 25 °C. The $[Mn^{III}(OMe)(dpaq)]^+$ complex reacts with TEMPOH and with phenolic substrates with O–H bond free energies up to 78.5 kcal/mol, and represents the only example of a monomeric Mn^{III}–OMe species that can activate phenolic O–H bonds. In contrast to that observed for the recently reported $[Mn^{III}(OH)(dpaq)]^+$ complex (Figure 1),[29] phenol oxidation by $[Mn^{III}(OMe)(dpaq)]^+$ does not show saturation behavior at high phenol concentrations, suggesting the absence of an accumulating intermediate. However, mechanistic studies suggest that $[Mn^{III}(OMe)(dpaq)]^+$ activates substrate O–H bonds by a CPET process. In light of the reactivity of $[Mn^{III}(OMe)(dpaq)]^+$ and other mid-valent Mn oxidants, a detailed discussion of thermodynamic and kinetic parameters dictating the feasibility of PCET is presented, and we discuss characteristic differences in the oxidative reactivity of mid-valent versus high-valent oxidants.

Experimental

All procedures, including the generation of organic substrates and kinetic experiments, were carried out under an argon atmosphere, unless otherwise stated. Acetonitrile, methanol and ether were degassed and dried using a Pure Solv Micro (2010) solvent purification system. These solvents were

degassed in air-tight solvent reservoirs (4 L) by bubbling Ar gas through the solvent for 20 min at room temperature. Acetonitrile and ether were dried using air-tight alumina columns, and methanol was dried using a drierite column. Anhydrous dichloromethane was purchased from Acros Organics (99.9% purity) and was degassed by four freeze-pump-thaw cycles using Schlenk techniques. All solvents were taken into an argon-filled glovebox immediately after dispensing from the solvent purification system, or following the freeze-pump-thaw cycles, and were stored in tightly-sealed Schlenk glassware. The purity of O_2 gas used was >99% and was further purified by passage through drierite and 5 Å molecular sieves prior to use. The amide-containing N_5 ligand H-dpaq, [Mn^{II}(dpaq)](OTf), and [Mn^{III}(OH)(dpaq)](OTf) were synthesized according to previously reported methods.[29, 31] TEMPOH and TEMPOD were also prepared according to literature procedures,[9, 32] and >99% deuteration of TEMPOD was confirmed by ^{1}H NMR experiments. All phenols, with >99% purity, were purchased from commercial sources.

Preparation of [Mn^{III}(OMe)(dpaq)](OTf) from [Mn^{II}(dpaq)](OTf) and Dioxygen

[Mn^{III}(OMe)(dpaq)](OTf) was generated by reacting a 2.5 mM [Mn^{II}(dpaq)](OTf) solution in MeOH with excess O_2 gas at room temperature. The formation of [Mn^{III}(OMe)(dpaq)](OTf) was monitored by electronic absorption spectroscopy, as it has characteristic features at 510 and 760 nm. These features show no significant shifts in terms of their energies when compared to [Mn^{III}(OH)(dpaq)](OTf) but are more defined for [Mn^{III}(OMe)(dpaq)](OTf) in methanol. In addition, a solvent-dependent broadening of the absorption features of [Mn^{III}(OMe)(dpaq)](OTf) was observed for spectra collected in MeCN. A representative formation reaction is as follows. A 2.5 mM [Mn^{II}(dpaq)](OTf) solution (2.9 mg in 2 mL of MeOH) was prepared under an inert atmosphere and transferred to a gas-tight cuvette sealed with a pierceable septum. An excess of O_2 gas was then delivered to the solution by means of a syringe, and the formation of [Mn^{III}(OMe)(dpaq)](OTf) was monitored by electronic absorption spectroscopy. The formation was complete in ~4000 min and the resulting dark red solution was evaporated to dryness under reduced pressure. The solid residue was then recrystallized using MeOH/ Et_2O (3.0 mg/ 98% yield). [Mn^{III}(OMe)(dpaq)](OTf) was further characterized by ESI-MS and magnetic susceptibility. ESI-MS: {[Mn^{III}(OMe)(dpaq)]$^+$} m/z = 468.1219 (calc. 468.1232; Figure S1). The solution phase magnetic susceptibly found was 5.53 μ_B (at 25 °C in CD_3CN), which compares well with the expected μ_{eff} = 4.89 μ_B for a monomeric high-spin d^4 system.[25] Cyclic voltammetry of [Mn^{III}(OMe)(dpaq)](OTf) was recorded in MeCN (12.4 mg in 10 mL) at 25 °C under an argon atmosphere. A 0.1 M $Bu_4N(PF_6)$ solution was used as the supporting electrolyte along with a glassy carbon working electrode, platinum auxiliary electrode and a AgCl/Ag reference electrode. Elemental analysis [Mn^{III}(OMe)(dpaq)](OTf) • 0.3 H_2O : $C_{25}H_{23.6}F_3MnN_5O_{5.3}S$ calc. (%): C 48.21, H 3.82, N 11.24; found (%): C 47.78, H 3.38, N 11.25.

Preparation of [Mn^{III}(OMe)(dpaq)](OTf) from [Mn^{III}(OH)(dpaq)](OTf)

A 2.5 mM solution of [Mn^{III}(OH)(dpaq)](OTf) (3.2 mg in 2 mL) was prepared as previously described,[29] and the solvent was removed under reduced pressure. The solid residue was stirred in MeOH for 10 min. The final solution color was deep red. The electronic absorption spectrum and ESI-MS of this solution are identical to that of [Mn^{III}(OMe)(dpaq)](OTf). This solution was then evaporated to dryness under reduced pressure and recrystallized using MeOH/ Et_2O. The final product was isolated as a solid in excellent yield (>98%). The resulting [Mn^{III}(OMe)(dpaq)](OTf) complex is quantitatively converted back to [Mn^{III}(OH)(dpaq)](OTf) (>98%) when dissolved in H_2O, as observed by ESI-MS experiments. Prominent ion peak in the mass spectrum of the resultant aqueous solution corresponds to m/z = 454.0902, as expected for [Mn^{III}(OH)(dpaq)]$^+$ (calc. m/z = 454.1076; Figure S1).

X-ray Diffraction Data Collection and Analysis for [Mn^{III}(OMe)(dpaq)](OTf)

Synthesis of [Mn^{III}(OMe)(dpaq)](OTf) on a large scale to obtain suitable material for X-ray crystallographic and kinetic experiments was carried out starting from [Mn^{III}(OH)(dpaq)](OTf). In this procedure, [Mn^{III}(OH)(dpaq)](OTf) (20 mg in 5 mL) was dissolved in MeOH and was stirred for 10 min. The conversion of [Mn^{III}(OH)(dpaq)](OTf) to [Mn^{III}(OMe)(dpaq)](OTf) was monitored by ESI-MS and electronic absorption spectroscopy. Upon complete conversion, the resulting solution was evaporated to dryness under reduced pressure, and the solid residue was repeatedly recrystallized by vapor diffusion using MeOH and Et_2O under ambient conditions. Red racemically-twinned crystals of the partially hydrated salt, [Mn(OCH$_3$)($C_{23}H_{20}N_5O$)]-[CF_3SO_3]$_2$, (1) are, at 100(2) K, orthorhombic, space group Pna2$_1$ – C_{2v}^9 (No. 33)[33] with a = 13.6388(4) Å, b = 26.1547(7) Å, c = 15.1412(4) Å, V = 5401.1(3) Å^3 and Z = 8 [Mn(OCH$_3$)($C_{23}H_{20}N_5O$)][CF_3SO_3] • 0.37 H_2O formula units (d_{calcd} = 1.533 g/cm^3; μ_a(CuKα) = 5.306 mm^{-1}). A full set of unique diffracted intensities (5238 frames with counting times of 2 to 5 seconds and an ω- or ϕ-scan width of 0.50°) was measured[34] for a single-domain specimen using monochromated CuKα radiation (λ= 1.54178 Å) on a Bruker Proteum Single Crystal Diffraction System equipped with Helios multilayer optics, an APEX II CCD detector and a Bruker MicroSTAR microfocus rotating anode X-ray source operating at 45 kV and 60 mA. Lattice constants were determined with the Bruker SAINT software package using peak centers for 9745 reflections. A total of 50470 integrated reflection intensities having 2θ(CuKα)< 140.02° were produced using the Bruker program SAINT;[35] 8511 of these were unique and gave R_{int} = 0.025. The data were corrected empirically for variable absorption effects using equivalent reflections; the relative transmission factors ranged from 0.715 to 1.000. The Bruker software package SHELXTL was used to solve the structure using "direct methods" techniques. All

stages of weighted full-matrix least-squares refinement were conducted using F_o^2 data with the SHELXTL Version 2010.3-0 software package.[36]

The asymmetric unit contains two cationic metal complexes, two anions, and a water molecule of crystallization. A substantial portion of the structure is disordered. The quinoline ring for the second metal complex is 56%/44% disordered with two slightly different orientations in the crystal. Mild restraints were eventually applied to the anisotropic thermal parameters for 13 of the disordered quinoline nonhydrogen atoms. The nonhydrogen bond lengths and angles for both orientations were restrained to have values similar to those for the quinoline ring of the first metal complex. *This disorder produces slightly elongated or flattened anisotropic thermal ellipsoids for atoms in these quinoline ligands.* The second triflate anion is also disordered with two slightly different (58%/42%) orientations and the water solvent molecule of crystallization is present only 74% of the time. Both orientations for the second (disordered) triflate anion were restrained to have bond lengths and angles similar to the first (ordered) triflate.

The final structural model incorporated anisotropic thermal parameters for all nonhydrogen atoms of both metal complexes and the ordered triflate as well as the water oxygen atom and the sulfur atoms for both orientations of the disordered triflate. All other nonhydrogen atoms were incorporated into the structural model with isotropic thermal parameters. The hydrogen atoms for the metal complexes were included in the structural model at idealized positions (sp^2- or sp^3-hybridized geometry and C–H bond lengths of 0.95 – 0.99 Å). The methoxy methyl groups were incorporated in the structural model as rigid groups (using idealized sp^3-hybridized geometry and C–H bond lengths of 0.98 Å) with idealized "staggered" geometry. The hydrogen atoms were assigned fixed isotropic thermal parameters with values 1.20 (nonmethyl) and 1.50 (methyl) times the equivalent isotropic thermal parameter of the carbon atom to which they are bonded.

A total of 826 parameters were refined using 211 restraints, 8511 data and weights of $w = 1/[\sigma^2(F_o^2) + (0.1429\ P)^2 + (13.9982\ P)]$, where $P = [F_O^2 + 2F_C^2]/3$. Final agreement factors at convergence for $[Mn(OCH_3)(C_{23}H_{20}N_5O)][CF_3SO_3] \cdot 0.37\ H_2O$ are: R_1(unweighted, based on F) = 0.075 for 8385 independent absorption-corrected "observed" reflections having $2\theta(CuK\alpha) < 140.02°$ and $I > 2\sigma(I)$; R_1(unweighted, based on F) = 0.076 and wR_2(weighted, based on F^2) = 0.213 for all 8511 independent absorption-corrected reflections having $2\theta(CuK\alpha) < 140.02°$. The largest shift/s.u. was 0.004 in the final refinement cycle. The final difference map had maxima and minima of 1.18 and -0.77 $e^-/Å^3$, respectively.

Kinetic Studies of [Mn^{III}(OMe)(dpaq)](OTf) with Substituted Phenols

For each kinetic experiment, a 1.25 mM $[Mn^{III}(OMe)(dpaq)]^+$ (1.5 mg, 2.5×10^{-3} mmol) solution was prepared in acetonitrile (2 mL) within an argon-filled glovebox, transferred to a gas-tight cuvette sealed with a pierceable

septum. Solutions of phenolic substrate were prepared in dichloromethane (300 µL) and sealed in a 4 mL glass vial with a pierceable septum. Then, the cuvette containing the $[Mn^{III}(OMe)(dpaq)]^+$ solution was inserted into a temperature-controlled cryostat (Unisoku), held at 50 °C, coupled to an Agilent 8453 UV/Visible spectrophotometer. Upon achieving thermal equilibrium (10 min), data collection was started, and 100 µL of the substrate solution was injected into the cuvette using a gas-tight syringe. Data collection times ranged from 300 to 6000 s. An aliquot of the final reaction mixture was analyzed by electron paramagnetic resonance (EPR) spectroscopy at 5 K. The rates of the reactions were calculated by applying the initial rate approximation in order to prevent any interference by side reactions at longer time scales. These initial rates (in absorbance units / time) were converted into s^{-1} units by using the extinction coefficient ($\varepsilon_{800} = 130\ M^{-1}\ cm^{-1}$) and initial concentration (1.25 mM) of $[Mn^{III}(OMe)(dpaq)]^+$. For reactions involving the 2,4,6-tri-*t*-butylphenol, the kinetic data were collected to five half-lives and fit directly to obtain a pseudo-first-order rate constant. In these cases, the directly obtained pseudo-first-order rate constants were identical, within error, to those obtained using the initial rate method. The rates of reactions involving 4-methoxy-2,6-di-*t*-butylphenol as the substrate were directly fit to obtain pseudo-first-order rate constants as they were significantly faster (data collection times 300 – 3000 s), and the data exhibited pseudo-first-order behavior up to at least five half-lives.

**Kinetic Studies of [Mn^{III}(OMe)(dpaq)](OTf) with TEMPOH(D)**

Similar to the kinetic experiments with phenols, a 1.25 mM $[Mn^{III}(OMe)(dpaq)]^+$ (1.5 mg, 2.5×10^{-3} mmol) solution was prepared in acetonitrile (2 mL) within an argon-filled glovebox, and was sealed in a gas-tight cuvette with a pierceable septum. The TEMPOH (or TEMPOD) solution was prepared in acetonitrile (100 µL) and sealed in a 300 µL glass vial with a pierceable septum. Data collection was started, and the TEMPOH (or TEMPOD) solution was added into the $[Mn^{III}(OMe)(dpaq)]^+$ solution using a gas-tight syringe. Data collection times ranged from 300 to 4000 s. Kinetic experiments at variable temperatures (-15 to 50 ℃) were performed following the same procedure as described, allowing the cuvette to achieve thermal equilibrium (10 min) in the cryostat, prior to the addition of the substrate. In order to confirm that substrate isotopic scrambling (*i.e.*, exchange of deuterium in TEMPOD with hydrogen due to trace H_2O) does not affect the H/D KIE, kinetic experiments were also performed where TEMPOD was dissolved in 1:1 MeCN:MeOD. The rates of reactions with added MeOD were identical, within error, to those without added MeOD ($6.50(7) \times 10^{-3}\ s^{-1}$ and $6.45(7) \times 10^{-3}\ s^{-1}$, respectively, for 100 equiv. of TEMPOD). All reactions involving TEMPOH (or TEMPOD) followed pseudo-first-order behavior up to at least five half-lives.

Results and Analysis

Formation of [Mn^{III}(OMe)(dpaq)](OTf) from Dioxygen

When treated with excess O_2 gas at 25 °C, the light orange colored methanol solution of [Mn^{II}(dpaq)](OTf) slowly changed its color to dark red, as new absorption features grew in at 510 (ε = 328 M^{-1} cm^{-1}) and 760 nm (ε = 130 M^{-1} cm^{-1}) (Figure 2; the extinction coefficients were obtained using recrystallized [Mn^{III}(OMe)(dpaq)](OTf)). These changes in the electronic absorption spectrum are consistent with the oxidation of the Mn^{II} center upon reacting with O_2. The final product of the oxygenation reaction, [Mn^{III}(OMe)(dpaq)](OTf), was isolated in an essentially quantitative yield of greater than 98%. The formation of [Mn^{III}(OMe)(dpaq)](OTf) from the oxygenation of a 2.5 mM [Mn^{II}(dpaq)](OTf) solution in methanol took over 33 hours to approach completion (Figure 2), which is significantly longer than that of the same reaction in MeCN (~40 min; see reference 29). A half-life ($t_{1/2}$) of 26 days was estimated for [Mn^{III}(OMe)(dpaq)](OTf) by monitoring the electronic absorption spectrum of a 1.25 mM acetonitrile solution at 25 °C. This is identical to the half-life observed previously for [Mn^{III}(OH)(dpaq)](OTf) under the same conditions.[29] At 50 °C, the same concentration of [Mn^{III}(OMe)(dpaq)](OTf) in MeCN has an appreciable self-decay rate of 2.5(2) $\times$ 10^{-5} s^{-1} at 50 °C, which corresponds to a half-life of 7.5(2) hours. [Mn^{III}(OH)(dpaq)](OTf) showed essentially no decay at 50 °C in MeCN.
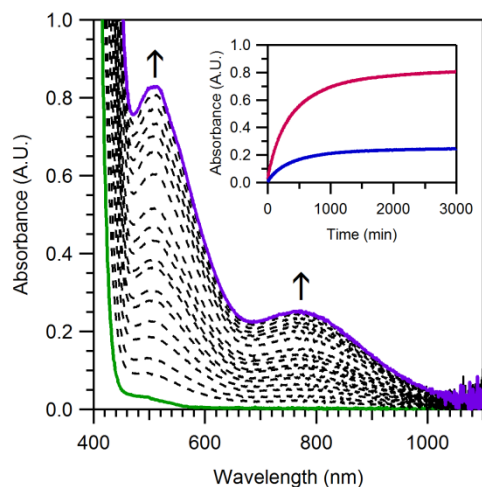

Figure 2. Electronic absorption spectra of 2.5 mM [Mn^{II}(dpaq)]$^+$ (solid green trace) upon the addition of excess O_2 at 25 °C in MeOH under argon. Inset: Time evolution of absorption signals at 510 and 760 nm from data collected every 5 min.

Structural and Physical Properties of [Mn^{III}(OMe)(dpaq)](OTf)

The X-ray structure of [Mn^{III}(OMe)(dpaq)](OTf) shows a six-coordinate Mn^{III} center with a distorted octahedral geometry (Figure 3), with the anionic amide ligand *trans* to the methoxide group. There are two molecules of [Mn^{III}(OMe)(dpaq)](OTf) within the asymmetric unit with very similar metric parameters; the metric parameters for the two

cationic units are in Table 1 and S2. The structure of [Mn^{III}(OMe)(dpaq)](OTf) is virtually identical to that of the previously reported [Mn^{III}(OH)(dpaq)](OTf) complex.[29] Most Mn−N distances are statistically indistinguishable from those of [Mn^{III}(OH)(dpaq)](OTf), with the exception of the Mn−N4 distance, which is shorter in [Mn^{III}(OMe)(dpaq)](OTf) (2.203(6) and 2.154(7) Å in the two cations) than in [Mn^{III}(OH)(dpaq)](OTf) (2.260(14) Å). The methoxide group in [Mn^{III}(OMe)(dpaq)](OTf) has Mn−O2 distances of 1.825(4) and 1.814(5) Å (Tables 1 and S2), comparable to those of other Mn^{III}−OMe distances reported in literature (1.836(5) and 1.814(7)).[25, 37] Two triflate ions and a water molecule are observed within the asymmetric unit as well but are not associated with the Mn centers (Mn−O(triflate) distances of 6.397 and 6.936 Å, and Mn−O(water) distances of 4.760 and 8.604 Å).
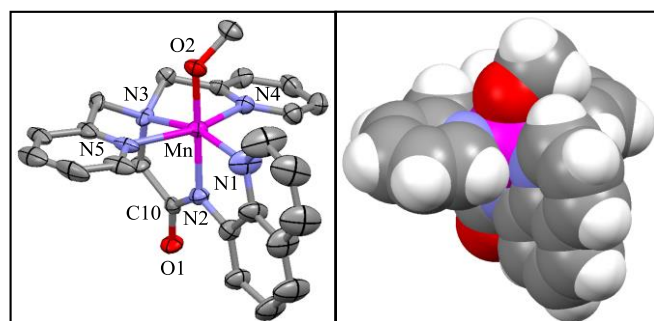
Figure 3. ORTEP (left) and space filling (right) diagrams of [Mn^{III}(OMe)(dpaq)](OTf). ORTEP diagram shows 50% probability thermal ellipsoids. Hydrogen atoms, non-coordinating triflate counteranions and the water molecule have been removed for clarity. Significant interatomic distances and angles are listed in Table 1.

Table 1. Bond Lengths and Angles for One of the Two [Mn^{III}(OMe)(dpaq)]$^+$ Cations in the Asymmetric Unit.^{a}

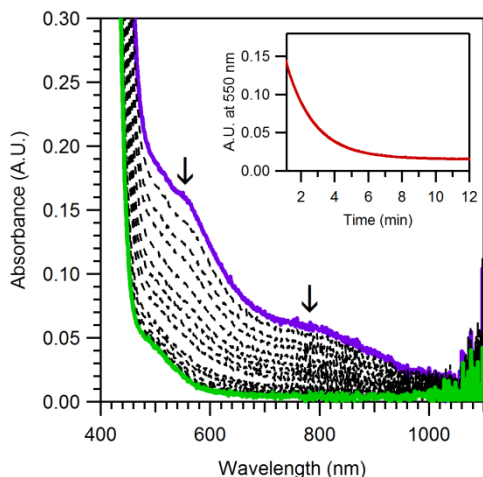|	[Mn^{III}(OMe)(dpaq)]$^+$ (A)		
Mn−O2	1.825(4)	O2−Mn−N2	177.9(3)
Mn−N2	1.979(5)	N4−Mn−N5	154.8(2)
Mn−N1	2.051(5)	N1−Mn−N3	161.7(2)
Mn−N3	2.175(5)	N4−Mn−N2	87.8(2)
Mn−N4	2.203(6)	N1−Mn−N2	80.0(2)
Mn−N5	2.212(6)	N3−Mn−N2	81.8(2)

^{a} Corresponding Metric Parameters for the Other Cation are in Table S2.

Cyclic voltammetric studies of [Mn^{III}(OMe)(dpaq)]$^+$ were performed in MeCN, and revealed an irreversible Mn^{III}/Mn^{II} couple at a cathodic peak potential ($E_{p,c}$) of -0.88 V vs Fc$^+$/Fc at a scan rate of 100 mV s^{-1} at 25 °C (Figure S2). Although it is unwise to make strong comparisons of this irreversible

reduction wave with the reversible or partially-reversible processes observed for the Mn^{III}/Mn^{II} couple of other mid-valent oxidants, including $[Mn^{III}(OH)(dpaq)]^+$, it is interesting that the $E_{p,c}$ of $[Mn^{III}(OMe)(dpaq)]^+$ is 0.22 V lower than the corresponding $E_{p,c}$ of $[Mn^{III}(OH)(dpaq)]^+$. The smaller reduction potential observed for $[Mn^{III}(OMe)(dpaq)]^+$ compared to $[Mn^{III}(OH)(dpaq)]^+$ is in contrast with the trend observed for several other M^{III}–OR oxidants,[25, 27, 28] but is consistent with the milder oxidizing ability of $[Mn^{III}(OMe)(dpaq)]^+$ (*vide infra*). In addition, in an electrochemical study of Mn^{III}–OR complexes supported by a phenol-containing N_4O^- ligand reported by Anxolabéhère-Mallart and co-workers, a slightly lower irreversible reduction potential was observed for the Mn^{III}–OMe complex compared to the analogous Mn^{III}–OH species.[37]

Separate frozen samples of 2 mM $[Mn^{III}(OMe)(dpaq)]^+$ in MeCN and 1:1 ethanol:methanol (the latter of which is a glassing solvent) were analyzed by EPR spectroscopy at 5 K. Neither sample showed features in either perpendicular or parallel modes. This is consistent with a monomeric Mn^{III} complex with a moderate to large zero-field splitting.

Reactivity of $[Mn^{III}(OMe)(dpaq)]^+$ with TEMPOH


Figure 4. Electronic absorption spectra of 1.25 mM $[Mn^{III}(OMe)(dpaq)]^+$ upon the addition of 100 equiv. TEMPOH at 25 ℃ in MeCN under argon. Inset: Decay of the 550 nm absorption signal from data collected every 0.3 s.

The PCET reactivity of $[Mn^{III}(OMe)(dpaq)]^+$ was investigated using TEMPOH as the substrate to permit comparison with other Mn^{III}–OR oxidants.[25, 29] Treatment of $[Mn^{III}(OMe)(dpaq)]^+$ with 100 equiv. of TEMPOH under an argon atmosphere in MeCN at 25 ℃ lead to the rapid disappearance of the electronic absorption bands of $[Mn^{III}(OMe)(dpaq)]^+$ (Figure 4). The final electronic absorption spectrum appears essentially identical to that of $[Mn^{II}(dpaq)](OTf)$ dissolved in MeCN, showing a very weak band at 510 nm. Using the intensity and the extinction coefficient of this band, the final yield of $[Mn^{II}(dpaq)]^+$ was calculated to be over 99%. The X-band EPR spectrum

(perpendicular-mode) of the final reaction mixture at 5 K shows an intense feature centered at $g = 2.04$ that is characteristic of the TEMPO radical (Figure S3). Together these data demonstrate that the reaction between TEMPOH and $[Mn^{III}(OMe)(dpaq)]^+$ approaches completion under these conditions, generating TEMPO radical and $[Mn^{II}(MeOH)(dpaq)]^+$.
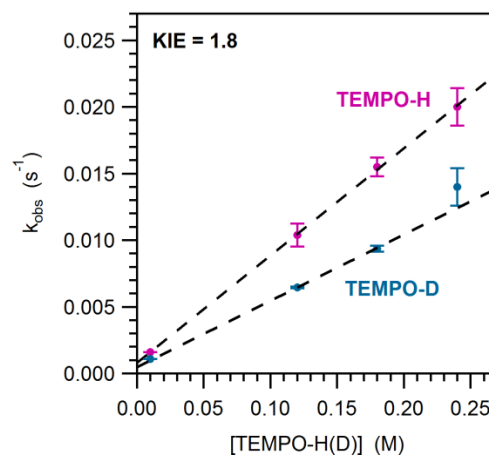
Figure 5. Pseudo-first order rate constants, k_{obs} (s^{-1}) versus TEMPOH and TEMPOD concentration for a 1.25 mM solution of $[Mn^{III}(OMe)(dpaq)]^+$ at 25 ℃. The second-order rate constant, k_2 (M^{-1}s^{-1}), was calculated from the linear correlation of the observed rate constant and substrate concentration.
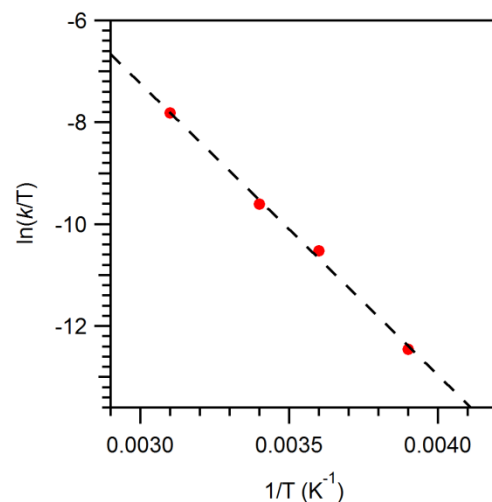
Figure 6. Eyring plot showing $\ln(k/T)$ versus $1/T$ (K^{-1}) for the reaction of 1.25 mM $[Mn^{III}(OMe)(dpaq)]^+$ with TEMPOH from -15 to 50 ℃ (258 to 323 K).

The reaction of $[Mn^{III}(OMe)(dpaq)]^+$ and TEMPOH was studied over a range of TEMPOH concentrations (10 – 200 equiv. with respect to initial $[Mn^{III}(OMe)(dpaq)]^+$ concentration), and the pseudo-first-order rate constants were observed to increase linearly with the concentration of TEMPOH (Figure 5). In all cases, the disappearance of $[Mn^{III}(OMe)(dpaq)]^+$ showed pseudo-first-order behavior up to at least five half-lives. A second-order rate constant of $8.0(1) \times 10^{-2}$ M^{-1} s^{-1} was calculated based on these data, which is slightly

lower than the rate observed for TEMPOH oxidation by $[Mn^{III}(OH)(dpaq)]^+$ $(1.3(1) \times 10^{-1}$ M^{-1} $s^{-1})$. Using the deuterated substrate, TEMPOD, a KIE of 1.8 was calculated for this PCET process, which suggests a rate-limiting O–H/D bond breaking step. Given the exceptionally high pK_a of TEMPOH in MeCN ($pK_a = 41$),[7] and the highly negative reduction potential of $[Mn^{III}(OMe)(dpaq)]^+$, these results are consistent with a rate-limiting CPET reaction. An Eyring analysis of the reaction between $[Mn^{III}(OMe)(dpaq)]^+$ and TEMPOH from -15 to 50 ℃ (258 to 323 K) yielded activation parameters $\Delta H^{\ddagger}$ and $\Delta S^{\ddagger}$ of 11.4(5) kcal/mol and -27(2) cal/mol K, respectively (Figure 6).

Reactivity of $[Mn^{III}(OMe)(dpaq)]^+$ with Phenols

$[Mn^{III}(OMe)(dpaq)]^+$ also reacted with 2,4,6-tri-t-butylphenol ($^{4-t-butyl}$ArOH) in MeCN at 50 ℃. The formation of the corresponding phenoxyl radical ($\lambda_{max} = 628$ nm; $\epsilon = 400(10)$ M^{-1} cm^{-1} in MeCN[38] at 25℃; see Figure 7) and the decay of $[Mn^{III}(OMe)(dpaq)]^+$ were concomitant, which suggests the absence of secondary reactions involving $[Mn^{III}(OMe)(dpaq)]^+$ and the radical. The phenoxyl radical was formed in ~75% yield relative to the initial $[Mn^{III}(OMe)(dpaq)]^+$ concentration, a yield similar to that previously reported for the reaction of $^{4-t-butyl}$ArOH with $[Mn^{III}(OH)(dpaq)]^+$.[29] The perpendicular-mode X-band EPR spectrum of the final products of $^{4-t-butyl}$ArOH oxidation provide evidence for the formation of the phenoxyl radical (Figure S3). The ~75% yield of the phenoxyl radical was observed regardless of the initial $[Mn^{III}(OMe)(dpaq)]^+$: $^{4-t-butyl}$ArOH ratio (Table S3).

When $[Mn^{III}(OMe)(dpaq)]^+$ was treated with an excess of $^{4-t-butyl}$ArOH (10 – 125 equiv.) in MeCN, the decay of $[Mn^{III}(OMe)(dpaq)]^+$ and the formation of $^{4-t-butyl}$ArO$^{\bullet}$ followed pseudo-first-order kinetics up to at least three half-lives. $[Mn^{III}(OMe)(dpaq)]^+$ exhibited linear dependence of the rate of the reaction (k_{obs}) on phenol concentration up to 0.15 M $^{4-t-butyl}$ArOH (Figure 8). The second order rate constant found from these data is $5.2(1) \times 10^{-3}$ M^{-1} s^{-1}. The y-intercept of the linear fit of k_{obs} versus $[^{4-t-butyl}$ArOH$]$ corresponds to a self-decay rate of $3.3(1) \times 10^{-5}$ s^{-1}, which is in good agreement with the observed self-decay rate of $[Mn^{III}(OMe)(dpaq)]^+$ of 2.5×10^{-5} s^{-1} in MeCN at 50℃ (*vide supra*).

The lack of rate saturation at high phenol concentrations is suggestive of a single-step reaction with no accumulating intermediates from a pre-equilibrium step. In addition, oxidation of $^{4-t-butyl}$ArOH by $[Mn^{III}(OMe)(dpaq)]^+$ in MeOH, instead of MeCN, at 50 ℃ shows a linear correlation between k_{obs} and $[^{4-t-butyl}$ArOH$]$ as well, with a second order rate constant of $3.7(1) \times 10^{-3}$ M^{-1} s^{-1} (Figure S4). The observation of similar rates in both protic and non-protic solvents for oxidation of the same substrate suggests the absence of charged intermediates during the course of the reaction.[27] Thus, the similar rates in MeOH and MeCN are supportive of a single step CPET process rather than a stepwise PCET, where the proton and electron transfer occur in separate kinetic steps.

To further investigate the mechanism of phenol oxidation, we explored the reactivity of $[Mn^{III}(OMe)(dpaq)]^+$ with other phenolic substrates, including 4-methoxy-2,6-di-t-butylphenol

($^{4-MeO}$ArOH), 4-methyl-2,6-di-t-butylphenol ($^{4-Me}$ArOH), 2,6-di-t-butylphenol ($^{4-H}$ArOH), and 4-cyano-2,6-di-t-butylphenol ($^{4-CN}$ArOH). A linear dependence between the oxidation rate and the O–H bond strength would provide stronger evidence for a CPET process for phenolic O–H oxidation by $[Mn^{III}(OMe)(dpaq)]^+$. With the exception of $^{4-CN}$ArOH, all of the phenols reacted with $[Mn^{III}(OMe)(dpaq)]^+$ to give phenoxyl radicals and Mn^{II} species, and in each case, a linear dependence between the rate of the reaction and the substrate concentration was observed (Figure S5). The second order rate constants calculated from these kinetic data are collected in Table 2. In the reaction of $[Mn^{III}(OMe)(dpaq)]^+$ with $^{4-CN}$ArOH (BDFE = 79 kcal/mol), the reaction did not approach completion, implying that the thermodynamic limit of the O–H bond oxidation by $[Mn^{III}(OMe)(dpaq)]^+$ lies around 79 kcal/mol.
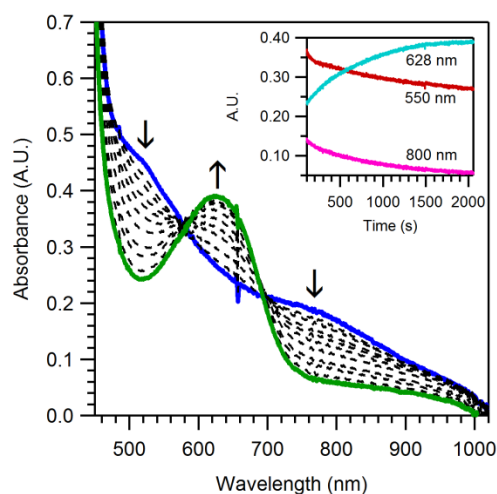
Figure 7. Electronic absorption spectra of 1.25 mM $[Mn^{III}(OMe)(dpaq)]^+$ upon the addition of 100 equiv. 2,4,6-tri-t-butylphenol ($^{4-t-butyl}$ArOH) at 50 ℃ in MeCN under argon. Inset: Time evolution of single-wavelength traces at 628, 550, and 800 nm.
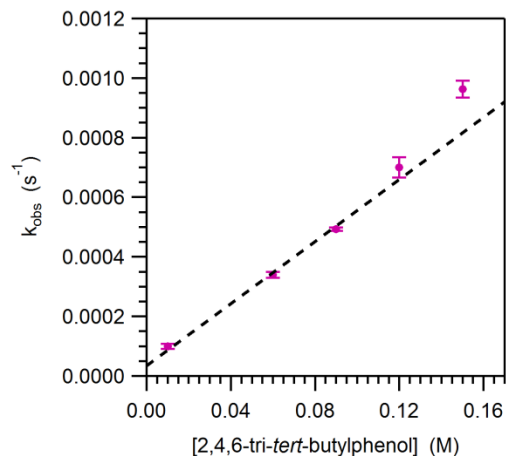

Figure 8. Observed pseudo-first-order rate constants (k_{obs}) as a function of $^{4-t-butyl}$ArOH concentration for $[Mn^{III}(OMe)(dpaq)]^+$.

Table 2. Rate Constants from Kinetic Experiments between $[Mn^{III}(OMe)(dpaq)]^+$ and O–H Bond Substrates in MeCN, and Substrate BDFE$_{O-H}$ Values.

substrate	k_2 (M^{-1} s^{-1})	BDFE$_{O-H}$ [a]
TEMPOH	$8.0(1) \times 10^{-2}$	66.5(1)
$^{4\text{-MeO}}$ArOH	1.1(1)	73.9(1)
$^{4\text{-Me}}$ArOH	$8.2(1) \times 10^{-3}$	76.0(1)
$^{4\text{-}t\text{-butyl}}$ArOH	$5.2(1) \times 10^{-3}$	77.1(1)
$^{4\text{-}t\text{-butyl}}$ArOH (MeOH) [b]	$3.7(1) \times 10^{-3}$	77.1(1)
$^{4\text{-H}}$ArOH	$1.4(1) \times 10^{-3}$	78.5(1)
$^{4\text{-CN}}$ArOH	[c]	79.0(1)

[a] kcal/mol; from Warren *et al.* (ref. 7) or determined following Waidman *et al.* (ref. 14). [b] MeOH was used as the solvent for this reaction. [c] The reaction of $[Mn^{III}(OMe)(dpaq)]^+$ with $^{4\text{-CN}}$ArOH did not go to completion.

An Evans-Polanyi plot generated using second-order rate constants of O–H bond oxidation reactions mediated by $[Mn^{III}(OMe)(dpaq)]^+$ is shown in Figure 9. This set of substrates comprise a reasonable range of substrate BDFEs (66 – 78.5 kcal/mol in MeCN),[39] and a linear dependence between the log of reaction rate versus BDFE of the substrate is observed with a slope of -0.2. In this analysis, the oxidation of $^{4\text{-MeO}}$ArOH displays a much faster rate than expected on the basis of its bond strength, and is a clear outlier (Figure 9). Importantly, the Polanyi slope obtained by excluding the data point for $^{4\text{-MeO}}$ArOH is still -0.2; thus, the deviation in the oxidation rate of $^{4\text{-MeO}}$ArOH does not affect the Polanyi slope. The slope seen for this series is smaller than expected from Marcus theory for a reaction with a small thermodynamic driving force (-0.5). Such small slopes have been seen for most mid-valent Mn and Fe oxidants (*vide infra*).[26-29]
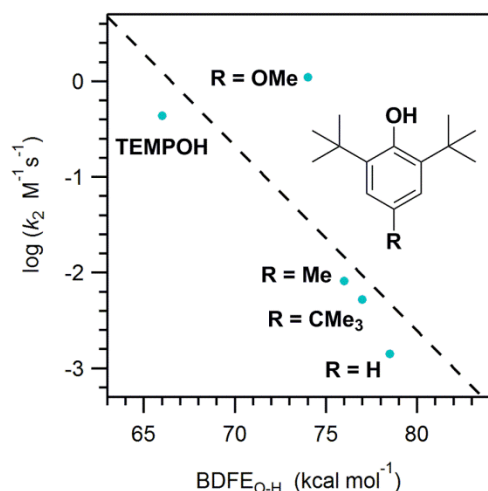
Figure 9. Evans-Polanyi plot of log of PCET rate (k_2) versus the BDFE of the substrate.

The C–H bond oxidation capability of $[Mn^{III}(OMe)(dpaq)](OTf)$ was also investigated using xanthene, which has a C–H BDFE of 73.3 kcal/mol in dimethysulfoxide. Treatment of a MeCN solution of $[Mn^{III}(OMe)(dpaq)](OTf)$ with xanthene at 50 °C led to an observed decay rate of the Mn^{III}–OMe complex indistinguishable to the self-decay rate at this temperature (Figure S6).[40] Thus, unlike the corresponding Mn^{III}–OH complex,[29] $[Mn^{III}(OMe)(dpaq)]^+$ does not appear to be capable of xanthene oxidation.

Discussion

Mn-dependent enzymes catalyze a range of biological processes, during which PCET reactions play a vital role.[1] Active sites in a number of these enzymes are known to contain mid-valent Mn oxidants.[41-45] Specifically, the active-site of Mn-lipoxygenase is presumed to contain a Mn^{III}–OH unit that initiates fatty acid oxidation by a PCET step.[27,45, 46] Support for this proposal comes from the H/D KIE of ~20 at 50 °C.[46] Notably, this KIE is significantly smaller than that of Fe-lipoxygenase (~56 at 30 °C),[47, 48] and, unlike that of Fe-lipoxyganese, the Mn-lipoxygenase H/D KIE is temperature-dependent, increasing to ~38 at 8 °C.[46] The basis for the different KIE behaviors of Fe- and Mn-lipoxygenases is currently unknown. In light of this and other biological examples, there have been several investigations of model complexes containing M^{III}–OR units (M = Mn or Fe).[25-29] Only a few of the synthetic M^{III}–OR complexes are known to mediate PCET reactions, but these studies have revealed interesting differences between mid-valent M^{III}–OR complexes and high-valent M$^{IV/V}$=O adducts.[25-29, 49] Most obviously, high-valent oxidants are capable of activating significantly stronger substrate bonds (up to 100 kcal/mol) than mid-valent oxidants (up to 80 kcal/mol). Although substrate oxidations of high-valent oxidants have been the subject of numerous detailed studies, understanding of PCET reactivity mediated by low-valent oxidants is still in its infancy.[49]

This present work describes the formation and PCET reactivity of the new Mn^{III}–OMe complex, $[Mn^{III}(OMe)(dpaq)]^+$. This complex is formed in quantitative yields by the reaction of $[Mn^{II}(dpaq)]^+$ with dioxygen in methanol. Previously reported $[Mn^{II}(dpaq)]^+$ represents a rare example of a monomeric Mn^{II} complex that can activate dioxygen in solution under ambient conditions to form a single product.[29] The mechanism of O_2 activation by $[Mn^{II}(dpaq)]^+$ is currently under investigation. Although synthetic Mn^{II} complexes that can activate dioxygen are unusual, the presence of an amido ligand, as in $[Mn^{II}(dpaq)]^+$, is known to significantly alter the electronic properties of the metal center.[50-55] $[Mn^{III}(OMe)(dpaq)]^+$ is remarkably stable in solution with a half-life of ~26 days in MeCN at 25 °C. In addition, a distinct property of this system is that $[Mn^{III}(OMe)(dpaq)]^+$ can be stoichiometrically generated by dissolving the previously reported $[Mn^{III}(OH)(dpaq)]^+$ complex in MeOH, and this reaction can be completely reversed when $[Mn^{III}(OMe)(dpaq)]^+$ is placed in water (Figure S1).

Table 3. Thermodynamic and Kinetic Parameters Related to PCET reactivity of Mn^{III}–OH and Mn^{III}–OMe Oxidants with TEMPOH in MeCN at 25 °C.

	[a][$Mn^{III}(OH)(dpaq)$]$^+$	[$Mn^{III}(OMe)(dpaq)$]$^+$	[b][$Mn^{III}(OH)(S^{Me2}N_4(tren))$]$^+$	[b][$Mn^{III}(OMe)(S^{Me2}N_4(tren))$]$^+$
k_2 (M^{-1} s^{-1})	1.3×10^{-1}	8.0×10^{-2}	2.1×10^{3}	3.6×10^{2}
conc. (mM)	1.25	1.25	0.5	0.5
E (M^{III}/M^{II})	-0.6 [d]	-0.88 [e]	-0.6 [d]	-0.45 [d]
pK_a M^{II}-O(H)R	NR [c]	NR [c]	21.2	≥ 16.2
BDFE M^{II}-O(H)R [f,g]	NR [c]	NR [c]	70.1	≥ 64.4
$\Delta H^{\ddagger}$ [g]	9.9(9)	11.4(5)	8.2	8.3
$\Delta S^{\ddagger}$ [h]	$-35(3)$	$-27(2)$	-25.5	-29
$\Delta G^{\ddagger}$ [g,i]	20.3(1.8)	19.5(1.1)	15.8	16.9

[a] Data taken from reference 29. [b] Data taken from reference 25. [c] Not reported. [d] Reduction potential ($E_{1/2}$) and [e] cathodic peak potential ($E_{p,c}$) vs Fc$^+$/Fc in volts at 25 °C in MeCN. [f] in MeCN. [g] in kcal/mol. [h] in cal/mol K. [i] at 25 °C.

PCET Mechanism of [$Mn^{III}(OMe)(dpaq)$]$^+$

[$Mn^{III}(OMe)(dpaq)$]$^+$ is capable of oxidizing substrate O–H bonds of BDFEs less than 79 kcal/mol. To date, this is the only Mn^{III}–OMe species reported to activate phenolic O–H bonds. Using this complex, we have performed the oxidation of a series of *para*-substituted-2,6-di-*tert*-butylphenols ($^{4-R}$ArOH) and TEMPOH (Table 2), which encompasses a reasonable range of substrate O–H BDFEs (66.5 – 78.5 kcal/mol). The Evans-Polanyi plot for O–H bond oxidation of these substrates by [$Mn^{III}(OMe)(dpaq)$]$^+$ shows a linear dependence of the log of O–H bond oxidation rates on the BDFE of the substrate O–H bond (Figure 9). This is suggestive of a CPET mechanism for O–H oxidation by [$Mn^{III}(OMe)(dpaq)$]$^+$. Furthermore, [$Mn^{III}(OMe)(dpaq)$]$^+$ reacts with TEMPOH, a substrate that is most likely to undergo CPET due to its remarkably high pK_a (41 in MeCN) and reduction potential (+0.71 V vs. Fc$^+$/Fc in MeCN).[7] The H/D KIE observed for this oxidation is 1.8, which is suggestive of a rate-limiting CPET. In addition, we carried out the oxidation of $^{4-t-butyl}$ArOH in both MeCN and MeOH, and these reactions proceed with similar second-order rates of 5.2(1) × 10^{-3} M^{-1} s^{-1} and 3.7(1) × 10^{-3} M^{-1} s^{-1} respectively (Figure S4). Such similar rates in both protic and non-protic solvents have been previously attributed to the absence of charged intermediates during the reaction, which suggests that sequential proton- and electron-transfer steps do not occur.[27] Finally, given the low $E_{p,c}$ for [$Mn^{III}(OMe)(dpaq)$]$^+$ (-0.88 V vs Fc$^+$/Fc in MeCN at 25 °C) and the potential for the PhO$^\bullet$/PhO$^-$ couple of $^{4-t-butyl}$ArOH (-0.70 V vs Fc$^+$/Fc in MeCN at 25 °C),[7] a stepwise PCET involving initial electron transfer between [$Mn^{III}(OMe)(dpaq)$]$^+$ and $^{4-t-butyl}$ArOH is energetically up-hill by at least 0.18 V. Taken together, these cumulative observations strongly support a CPET process for [$Mn^{III}(OMe)(dpaq)$]$^+$-mediated O–H bond oxidation.

The thermodynamic driving force for these CPET processes is defined as the difference in O–H BDFE of the reduced-protonated form of the oxidant (M^{II}–O(H)R in Scheme 1; M = Mn or Fe) and that of the substrate being oxidized. When both the pK_a of the M^{II}–O(H)R species and E^o of the M^{III}/M^{II} couple are known, the BDFE of the metal oxidant can be calculated using the Bordwell relationship (*vide supra*). Although we were able to obtain an $E_{p,c}$ of -0.88 V (vs Fc$^+$/Fc) for the Mn^{III}/Mn^{II} couple of [$Mn^{III}(OMe)(dpaq)$]$^+$ (Figure S2), all attempts in determining the pK_a of the M^{II}–O(H)R form of this oxidant were unsuccessful.[56] We have encountered similar difficulties in determining the pK_a for [$Mn^{II}(OH_2)(dpaq)$]$^+$. Consequently, the BDFEs of [$Mn^{II}(MeOH)(dpaq)$]$^+$ and [$Mn^{II}(OH_2)(dpaq)$]$^+$ are not known.

In contrast, the thermodynamic driving forces for PCET reactions by other Mn^{III}–OR adducts have been determined using experimental BDFEs of the M^{II}–O(H)R species.[25-28] For example, the BDFE of [$Mn^{II}(OH_2)(S^{Me2}N_4(tren))$]$^+$ was determined using a modified Bordwell relationship,[25] and was found to be 70.1 kcal/mol in MeCN (74.0 kcal/mol in H$_2$O). In that study, [$Mn^{III}(OH)(S^{Me2}N_4(tren))$]$^+$ exhibited a E^o of -0.60 V (vs Fc$^+$/Fc), and the corresponding Mn^{II}–OH$_2$ species had a pK_a of 21.2 (Table 3). The related Mn^{III}–OMe complex exhibited a E^o of -0.45 V (vs Fc$^+$/Fc), but the pK_a of the Mn^{III}–O(H)Me form could not be precisely defined (a lower limit of 16.2 was estimated). Based on these values, the M^{II}–OH$_2$ complex has a stronger O–H bond by at most 5.6 kcal/mol compared to the M^{II}–O(H)Me species (Table 3).[25] As a consequence of these weak BDFEs, [$Mn^{III}(OH)(S^{Me2}N_4(tren))$]$^+$ and [$Mn^{III}(OMe)(S^{Me2}N_4(tren))$]$^+$ were only able to oxidize TEMPOH. In contrast, Stack and Goldsmith reported a BDFE

Table 4. Comparison of H/D KIEs and Polanyi slopes for O−H Activation by Mid-valent vs High-valent Oxidants

Oxidant	Solvent	Polanyi slope	H/D KIE	T (°C)
mid-valent oxidants				
$[Mn^{III}(OMe)(dpaq)]^+$	MeCN	-0.2	1.8 [a]	25
$[Mn^{III}(OH)(dpaq)]^+$	MeCN	-0.07	1.8 [a], 1.4 [b]	25, 50
$[Mn^{III}(OMe)(S^{Me2}N_4(tren))]^+$	MeCN	NR [d]	2.1 [a]	25
$[Mn^{III}(OH)(S^{Me2}N_4(tren))]^+$	MeCN	NR [d]	3.1 [a]	25
$[Fe^{III}(OMe)(PY5)]^+$	MeCN	NR [d]	2.0 [b]	25
high-valent oxidants				
$[(TBP_8Cz)Mn^V(O)]$	DCM	-0.39	5.9 [b]	23
$[Mn^{IV}(salen)(OH)]$	DCM	-0.59 [e]	9.5 [c]	-70
$[Fe^{IV}(O)(TMC)(N_3)]^-$	MeCN	-0.36	NR [d]	25
$[Fe^{IV}(O)(TMC)(OOCCF_3)]^-$	MeCN	-0.42	NR [d]	25
$[Fe^{IV}(O)(TMC)(NCCH_3)]^-$	MeCN	-0.55	NR [d]	25
$[Fe^{IV}(\beta\text{-BPMCN})(OO^tBu)(OH)]^{2+}$	PrCN	-0.4 [e]	2.0 [b]	-70

H/D KIE was studied using [a] TEMPOH, [b] 4-t-butyl ArOH, and [c] 4-H ArOH as the O−H bond substrate. [d] Not reported. [e] Polanyi slopes were not reported; we calculated the slope using the reported kinetic data in refs. 55 and 57.

of 82 kcal/mol in MeCN for the $[Mn^{II}(OH_2)(PY5)]^{2+}$ complex, and, as a result, the $[Mn^{III}(OH)(PY5)]^{2+}$ oxidant was capable of oxidizing moderately strong C−H bonds, including that of toluene (C−H BDFE of 87 kcal/mol in MeCN),[7] with a second-order rate constant of $2.2(5) \times 10^{-3}$ M^{-1} s^{-1}.[26] Therefore, the current examples of Mn^{III}−OH complexes reveal that, even with the same metal and −OR ligand, the BDFE of the metal oxidant can vary considerably (12 kcal/mol) as a function of the supporting ligand. Although the BDFEs are not known for the reduced, protonated forms of $[Mn^{III}(OMe)(dpaq)]^+$ and $[Mn^{III}(OH)(dpaq)]^+$, these complexes show reactivity intermediate between the $S^{Me2}N_4(tren)$- and PY5-supported systems. That is, unlike the $[Mn^{III}(OR)(S^{Me2}N_4(tren))]^+$ complexes, the $[Mn^{III}(OR)(dpaq)]^+$ oxidants can oxidize phenolic O−H bonds, but cannot oxidize the stronger C−H bonds that the $[Mn^{III}(OH)(PY5)]^+$ complex readily attacks.

Rates and Activation Parameters for O−H Bond Oxidation by Mid-valent Mn Oxidants

TEMPOH is commonly used as weak O−H bond substrate (BDFE = 66.5 kcal/mol in MeCN) in metal-mediated PCET processes and provides a good point of comparison for the reactivity of Mn^{III}−OR oxidants (Table 3). $[Mn^{III}(OMe)(dpaq)]^+$ oxidizes TEMPOH at a second-order rate of 8.0×10^{-2} M^{-1} s^{-1} in MeCN at 25 °C, which is very similar to that of

$[Mn^{III}(OH)(dpaq)]^+$ (1.3×10^{-1} M^{-1} s^{-1}). The enthalpy of activation ($\Delta H^\ddagger$) for TEMPOH oxidation by $[Mn^{III}(OMe)(dpaq)]^+$ is 11.4(5) kcal/mol, marginally higher than that observed for $[Mn^{III}(OH)(dpaq)]^+$ (9.9(9) kcal/mol). In contrast, $[Mn^{III}(OMe)(dpaq)]^+$ shows a smaller entropic barrier to TEMPOH oxidation when compared to $[Mn^{III}(OH)(dpaq)]^+$ ($T\Delta S^\ddagger = 8.0(6)$ and 10.4(9) kcal/mol at 25 °C, respectively). As a net result of these changes in $\Delta H^\ddagger$ and $T\Delta S^\ddagger$, $[Mn^{III}(OMe)(dpaq)]^+$ and $[Mn^{III}(OH)(dpaq)]^+$ have similar free energies of activation ($\Delta G^\ddagger$) for TEMPOH oxidation at 25 °C (19.5(1.1) and 20.3(1.8) kcal/mol respectively). This is consistent with the very similar second-order rate constants at this temperature (Table 3).

On the other hand, the $\Delta G^\ddagger$ (25 °C) for TEMPOH oxidation by $[Mn^{III}(OMe)(S^{Me2}N_4(tren))]^+$ and $[Mn^{III}(OH)(S^{Me2}N_4(tren))]^+$ were found to be 16.9 and 15.8 kcal/mol respectively, substantially lower than those of the $[Mn^{III}(OR)(dpaq)]^+$ complexes. This is in line with the 10^4-greater rate of TEMPOH oxidation by the $S^{Me2}N_4(tren)$-supported complexes (Table 3). The 1.1 kcal/mol difference between the $\Delta G^\ddagger$ values of $[Mn^{III}(OMe)(S^{Me2}N_4(tren))]^+$ and $[Mn^{III}(OH)(S^{Me2}N_4(tren))]^+$ results in the Mn^{III}−OMe complex having a rate of TEMPOH oxidation an order of magnitude slower than that of the Mn^{III}−OH complex (3.6×10^2 and 2.1×10^3 M^{-1}s^{-1}, respectively).[25] Notably, the enthalpic ($\Delta H^\ddagger$) contribution to the

$\Delta G^{\ddagger}$ values of $[Mn^{III}(OMe)(S^{Me2}N_4(tren))]^+$ and $[Mn^{III}(OH)(S^{Me2}N_4(tren))]^+$ are virtually identical (Table 3). Thus, the more sluggish reactivity of $[Mn^{III}(OMe)(S^{Me2}N_4(tren))]^+$ is due to the larger entropy of activation (Table 3). However, the smaller $\Delta G^{\ddagger}$ for TEMPOH oxidation by $[Mn^{III}(OR)(S^{Me2}N_4(tren))]^+$ complexes in comparison with $[Mn^{III}(OR)(dpaq)]^+$ oxidants is intriguing, given that it solely reflects differences between the dpaq and $S^{Me2}N_4(tren)$ supporting ligands (Figure 1).

When comparing the phenol oxidation rates of $[Mn^{III}(OMe)(dpaq)]^+$ and $[Mn^{III}(OH)(dpaq)]^+$, the most significant difference is that the former complex lacks the rate saturation behavior at high phenol concentrations.[29] The saturation behavior of $[Mn^{III}(OH)(dpaq)]^+$ was proposed to be due to the equilibrium formation of a precursor complex prior to the rate-determining CPET step. This precursor complex was proposed to be a hydrogen-bonded adduct between the phenolic substrate and the $Mn^{III}-OH$ unit of $[Mn^{III}(OH)(dpaq)]^+$. The formation of a similar adduct might be disfavored for $[Mn^{III}(OMe)(dpaq)]^+$ due to steric clash between the methyl moiety and the bulky phenol substrates. For most of the phenols, the K_{eq} for precursor complex formation with $[Mn^{III}(OH)(dpaq)]^+$ was ~20, which corresponds to a small free energy of reaction of ~2 kcal/mol. Thus, a subtle steric or electronic effect in the $[Mn^{III}(OMe)(dpaq)]^+$ system could be expected to impact the equilibrium position such that the pre-equilibrium step is no longer observed.

KIEs and Polanyi Slopes of Mid-valent Oxidants

In comparison with high-valent oxidants, the H/D KIEs and the Polanyi slopes for O–H bond oxidations by mid-valent oxidants display notable differences, as summarized in Table 4. The KIEs for O–H bond oxidation reactions of mid-valent M–OR oxidants are smaller (~2 – 3)[25, 29] than those of high-valent oxo and hydroxo oxidants (~5 – 10),[23, 57, 58] with the exception of the $[Fe^{IV}(\beta\text{-BPMCN})(OO^tBu)(OH)]^{2+}$ oxidant.[59] For example, the H/D KIE observed for [4-t-butyl]ArOH oxidation by $[Mn^{III}(OH)(dpaq)]^+$ is remarkably small (1.4),[29] while the high-valent $Mn^V\equiv O$ complex, $[(TBP_8Cz)Mn^V(O)]$, has been shown to carry out the same substrate oxidation at a similar temperature with a larger KIE of 5.9.[23]

Moreover, according to Marcus theory, a Polanyi slope of -0.5 is expected for a process with a small thermodynamic driving force and a transition state position mid-way between reactants and products.[60] The Polanyi slopes observed for O–H oxidation reactions of mid-valent oxidants range between -0.07[29] and -0.2,[61] which is significantly smaller than the expected value. This is in contrast with high-valent oxidants that oxidize substrate O–H bonds with a Polanyi slope of -0.4 to -0.8.[20, 23, 57-59] Each Polanyi study listed in Table 4 is based on *para*-substitued-2,6-di-*tert*-butylphenols as O–H substrates. Irrespective of the identity of the metal (Mn or Fe), high-valent oxidants show slopes closer to the expected value of -0.5. Generally, a Polanyi slope of <0.5 indicates an early transition state that resembles the reactants,[60] with a rate less sensitive to the driving force of the reaction. It is an open question

therefore, whether the lower sensitivity of PCET rates to the driving force of the reaction is a characteristic property of these mid-valent oxidants, and if they go through an early transition state regardless of the identity of the substrate. The small KIE values observed for these oxidants could also be a consequence of this phenomenon.

Conclusions and Outlook

Designing metal oxidants with well-tuned properties for rapid, selective PCET is a desirable goal in synthetic chemistry, as such oxidants could be of significant benefit in industry, as well as in biomimetic studies. Among other metal oxidants, mid-valent M−OR adducts exhibit the potential for good tunability in their PCET reactivities, as both E^o and pK_a can be controlled by changing the R group in the M−OR unit, or through modification of the supporting ligand. For example, the variation in Mn^{III}/Mn^{II} potentials with respect to the properties of the supporting ligands is observed in the series of $Mn^{III}-OH$ complexes supported by neutral PY5 (+0.17 V vs Fc+/Fc), monoanionic $S^{Me2}N_4(tren)$ and dpaq (-0.60 V vs Fc+/Fc for both), and trianionic H_31^{3-} (H_31^{3-} = [[tris(*N'-tert*-butylureaylato)N-ethyl]aminato]) ligands (-1.51 V vs Fc+/Fc).[25, 26, 62] Also, the pK_a of the oxidant can be altered utilizing supporting ligands and −OR ligand properties, as seen in the $[Mn^{III}(OR)(S^{Me2}N_4(tren))]^+$ series of complexes (Table 3).[25] As a result of these differences, a range of O−H BDFEs is observed for $M^{II}-OH_2$ species derived from $M^{III}-OH$ oxidants (12 kcal/mol), along with large differences in substrate oxidation rates (10^4-fold for TEMPOH as substrate; see Table 3). However, additional work on mid-valent oxidants is warranted to gain further insight into the specific geometric and electronic factors governing their PCET reactivities.

Acknowledgements

Notes and references

Department of Chemistry and Center for Environmentally Beneficial Catalysis, University of Kansas, Lawrence, Kansas 66045.

1. J. M. Mayer and I. J. Rhile, *Biochimica et Biophysica Acta (BBA) - Bioenergetics*, 2004, **1655**, 51-58.

2. Y. Umena, K. Kawakami, J.-R. Shen and N. Kamiya, *Nature (London, U. K.)*, 2011, **473**, 55-60.

3. C. Tommos and G. T. Babcock, *Acc. Chem. Res.*, 1998, **31**, 18-25.

4. K. L. Westphal, C. Tommos, R. I. Cukier and G. T. Babcock, *Current Opinion in Plant Biology*, 2000, **3**, 236-242.

5. S. Kim, J. Liang and B. A. Barry, *Proc. Natl. Acad. Sci. U. S. A.*, 1997, **94**, 14406-14411.

6. G. T. Babcock, 1995.

7. J. J. Warren, T. A. Tronic and J. M. Mayer, *Chem. Rev. (Washington, DC, U. S.)*, 2010, **110**, 6961-7001.

8. M. H. V. Huynh and T. J. Meyer, *Chem. Rev. (Washington, DC, U. S.)*, 2007, **107**, 5004-5064.

9. E. A. Mader, E. R. Davidson and J. M. Mayer, *J. Am. Chem. Soc.*, 2007, **129**, 5153-5166.

10. E. A. Mader, V. W. Manner, T. F. Markle, A. Wu, J. A. Franz and J. M. Mayer, *J. Am. Chem. Soc.*, 2009, **131**, 4335-4345.

11. E. A. Mader and J. M. Mayer, *Inorg. Chem.*, 2010, **49**, 3685-3687.

12. V. W. Manner and J. M. Mayer, *J. Am. Chem. Soc.*, 2009, **131**, 9874-9875.

13. J. M. Mayer, *Acc. Chem. Res.*, 2010, **44**, 36-46.

14. C. R. Waidmann, X. Zhou, E. A. Tsai, W. Kaminsky, D. A. Hrovat, W. T. Borden and J. M. Mayer, *J. Am. Chem. Soc.*, 2009, **131**, 4729-4743.

15. J. J. Warren and J. M. Mayer, *J. Am. Chem. Soc.*, 2008, **130**, 2774-2776.

16. J. J. Warren and J. M. Mayer, *J. Am. Chem. Soc.*, 2011, **133**, 8544-8551.

17. J. J. Warren, A. R. Menzeleev, J. S. Kretchmer, T. F. Miller, H. B. Gray and J. M. Mayer, *J. Phys. Chem. Lett.*, 2013, **4**, 519-523.

18. J. P. Layfield and S. Hammes-Schiffer, *Chem. Rev. (Washington, DC, U. S.)*, 2013, **114**, 3466-3494.

19. Alternatively, HAT and CPET have respectively been attributed to electronically adiabatic and nonadiabatic proton transfer, as described by Hammes-Schiffer and co-workers (see reference 18).

20. C. V. Sastri, J. Lee, K. Oh, Y. J. Lee, J. Lee, T. A. Jackson, H. Hirao, L. Que, Jr., S. Shaik and W. Nam, *Proc. Natl. Acad. Sci. U. S. A.*, 2007, **104**, 19181-19186.

21. D. F. Leto, R. Ingram, V. W. Day and T. A. Jackson, *Chem. Commun. (Cambridge, U. K.)*, 2013, **49**, 5378-5380.

22. C. Krebs, D. Galonić Fujimori, C. T. Walsh and J. M. Bollinger, *Acc. Chem. Res.*, 2007, **40**, 484-492.

23. D. E. Lansky and D. P. Goldberg, *Inorg. Chem.*, 2006, **45**, 5119-5125.

24. D. Wang, M. Zhang, P. Bühlmann and L. Que, Jr., *J. Am. Chem. Soc.*, 2010, **132**, 7638-7644.

25. M. K. Coggins, L. M. Brines and J. A. Kovacs, *Inorg. Chem.*, 2013, **52**, 12383-12393.

26. C. R. Goldsmith, A. P. Cole and T. D. P. Stack, *J. Am. Chem. Soc.*, 2005, **127**, 9904-9912.

27. C. R. Goldsmith, R. T. Jonas and T. D. P. Stack, *J. Am. Chem. Soc.*, 2001, **124**, 83-96.

28. C. R. Goldsmith and T. D. P. Stack, *Inorg. Chem.*, 2006, **45**, 6048-6055.

29. G. B. Wijeratne, B. Corzine, V. W. Day and T. A. Jackson, *Inorg. Chem.*, 2014, **53**, 7622-7634.

30. F. G. Bordwell, J. Cheng, G. Z. Ji, A. V. Satish and X. Zhang, *J. Am. Chem. Soc.*, 1991, **113**, 9790-9795.

31. Y. Hitomi, K. Arakawa, T. Funabiki and M. Kodera, *Angew. Chem., Int. Ed.*, 2012, **51**, 3448-3452.

32. A. Wu, E. A. Mader, A. Datta, D. A. Hrovat, W. T. Borden and J. M. Mayer, *J. Am. Chem. Soc.*, 2009, **131**, 11985-11997.

33. V. A. International Tables for Crystallography, 4th ed., Kluwer: Boston (1996).

34. E. C. P. Data Collection: SMART Software in APEX2 v2010.3-0 Suite. Bruker-AXS, Madison, WI 53711-5373 USA.

35. E. C. P. Data Reduction: SAINT Software in APEX2 v2010.3-0 Suite. Bruker-AXS, Madison, WI 53711-5373 USA.

36. E. C. P. Refinement: SHELXTL v2010.3-0. Bruker-AXS, Madison, WI 53711-5373 USA.

37. S. E. Ghachtouli, R. Guillot, A. Aukauloo, P. Dorlet, E. Anxolabéhère-Mallart and C. Costentin, *Inorg. Chem.*, 2012, **51**, 3603-3612.

38. V. W. Manner, T. F. Markle, J. H. Freudenthal, J. P. Roth and J. M. Mayer, *Chem. Commun. (Cambridge, U. K.)*, 2008, 256-258.

39. To investigate if the mixed solvent system used for phenol oxidation reactions significantly impacts the kinetic data, a set of kinetic experiments were performed where the oxidation of TEMPOD was studied in the 20:1 MeCN:DCM solvent mixture used in the phenol oxidation experiments. TEMPOD oxidation in the mixed solvent resulted in essentially identical oxidation rates as observed in pure MeCN ($6.53(4) \times 10^{-3}$ s^{-1} and $6.45(7) \times 10^{-3}$ s^{-1}, respectively, for 100 equiv. of TEMPOD).

40. Upon the addition of 250 equiv. of xanthene at 50 ºC, the electronic absorption features of [Mn^{III}(OMe)(dpaq)]$^+$ in MeCN slowly decays over several hours. At the end of 25 hours, 10% of the [Mn^{III}(OMe)(dpaq)]$^+$ complex had been consumed (Figure S6). However, the observed decay rate (4.7×10^{-5} s^{-1}, determined using the initial rate method), was very similar the self-decay rate under these conditions (2.5×10^{-5} s^{-1}).

41. J. P. McEvoy and G. W. Brudvig, *Chem. Rev. (Washington, DC, U. S.)*, 2006, **106**, 4455-4483.

42. A.-F. Miller, *Curr. Opin. Chem. Biol.*, 2004, **8**, 162-168.

43. L. E. Grove and T. C. Brunold, *Comments Inorg. Chem.*, 2008, **29**, 134-168.

44. C. Su and E. H. Oliw, *J. Biol. Chem.*, 1998, **273**, 13072-13079.

45. C. Su, M. Sahlin and E. H. Oliw, *J. Biol. Chem.*, 2000, **275**, 18830-18835.

46. A. Wennman, S. Karkehabadi and E. H. Oliw, *Arch. Biochem. Biophys.*, 2014, **555–556**, 9-15.

47. M. H. Glickman and J. P. Klinman, *Biochemistry*, 1995, **34**, 14077-14092.

48. E. N. Segraves and T. R. Holman, *Biochemistry*, 2003, **42**, 5236-5243.

49. T. R. Porter and J. M. Mayer, *Chem. Sci.*, 2014, **5**, 372-380.

50. K. J. Young, M. K. Takase and G. W. Brudvig, *Inorg. Chem.*, 2013, **52**, 7615-7622.

51. Y. Hitomi, K. Arakawa and M. Kodera, *Chem. Commun. (Cambridge, U. K.)*, 2014, **50**, 7485-7487.

52. A. A. Eroy-Reveles, Y. Leung, C. M. Beavers, M. M. Olmstead and P. K. Mascharak, *J. Am. Chem. Soc.*, 2008, **130**, 4447-4458.

53. R. Gupta, C. E. MacBeth, V. G. Young and A. S. Borovik, *J. Am. Chem. Soc.*, 2002, **124**, 1136-1137.

54. C. E. MacBeth, R. Gupta, K. R. Mitchell-Koch, V. G. Young, G. H. Lushington, W. H. Thompson, M. P. Hendrich and A. S. Borovik, *J. Am. Chem. Soc.*, 2004, **126**, 2556-2567.

55. Z. Shirin, A. S. Borovik and V. G. Young Jr, *Chem. Commun. (Cambridge, U. K.)*, 1997, 1967-1968.

56. The determination of the pK_a by titrating [Mn^{III}(OMe)(dpaq)]$^+$ with various acids (HCl and HClO$_4$) was attempted in MeCN. Unfortunately, [Mn^{III}(OMe)(dpaq)]$^+$ reacts rapidly with acids to generate a Mn^{II} species, as determined from EPR spectroscopy. On the basis of these observations, we presume that [Mn^{III}(MeOH)(dpaq)]$^+$ is highly unstable, and decays by an unknown mechanism. Consequently, the determination of the pK_a of [Mn^{II}(MeOH)(dpaq)]$^+$ was not feasible by titrating [Mn^{III}(OMe)(dpaq)]$^+$ with acid.

57. T. Kurahashi, A. Kikuchi, Y. Shiro, M. Hada and H. Fujii, *Inorg. Chem.*, 2010, **49**, 6664-6672.

58. D. T. Y. Yiu, M. F. W. Lee, W. W. Y. Lam and T.-C. Lau, *Inorg. Chem.*, 2003, **42**, 1225-1232.

59. A. T. Fiedler and L. Que, Jr., *Inorg. Chem.*, 2009, **48**, 11038-11047.

60. J. M. Mayer, in *Biomimetic Oxidations Catalyzed by Transition Metal Complexes* ed. B. Meunier, Imperial College Press, London, 2000, pp. 1-43.

61. The only examples for Polanyi studies of O-H bond oxidation by mid-valent oxidants are found in our work on [Mn^{III}(OH)(dpaq)]$^+$ and [Mn^{III}(OMe)(dpaq)]$^+$. Thus, it should be noted that this range of Polanyi slopes comes from a limited set of oxidants. However, for C-H oxidation reactions of Mn and Fe mid-valent oxidants of Stack and co-workers, small Polanyi slopes were observed that ranged between -0.1 and -0.2 (see references 26, 27 and 28).

62. R. Gupta and A. S. Borovik, *J. Am. Chem. Soc.*, 2003, **125**, 13234-13242.